Dependence on fiber Fabry-Pérot tunable filter characteristics in an all-fiber swept-wavelength laser for use in an optical coherence tomography system

Justin L. Stay[1], Dustin Carr[1], Steve Ferguson[1], Todd Haber[1], Robert Jenkins[1], and Joel Mock[1]

[1]Micron Optics, Inc., 1852 Century Place, Atlanta, GA, USA

ABSTRACT

Optical coherence tomography (OCT) has become a useful and common diagnostic tool within the field of ophthalmology. Although presently a commercial technology, research continues in improving image quality and applying the imaging method to other tissue types. Swept-wavelength lasers based upon fiber ring cavities containing fiber Fabry-Pérot tunable filters (FFP-TF), as an intracavity element, provide swept-source optical coherence tomography (SS-OCT) systems with a robust and scalable platform. The FFP-TF can be fabricated within a large range of operating wavelengths, free spectral ranges (FSR), and finesses. To date, FFP-TFs have been fabricated at operating wavelengths from 400 nm to 2.2 μm, FSRs as large as 45 THz, and finesses as high as 30 000. The results in this paper focus on presenting the capability of the FFP-TF as an intracavity element in producing swept-wavelength lasers sources and quantifying the trade off between coherence length and sweep range. We present results within a range of feasible operating conditions. Particular focus is given to the discovery of laser configurations that result in maximization of sweep range and/or power. A novel approach to the electronic drive of the PZT-based FFP-TF is also presented, which eliminates the need for the existence of a mechanical resonance of the optical device. This approach substantially increases the range of drive frequencies with which the filter can be driven and has a positive impact for both the short all-fiber laser cavity (presented in this paper) and long cavity FDML designs as well.

Keywords: optical coherence tomography, tunable filter, optical frequency domain imaging, Fabry-Pérot, swept wavelength laser, high speed swept laser

1. LASER RING AND INTERLEAVER ARCHITECTURE

Recently there has been interest in a novel laser configuration for generating high speed swept-wavelength sources for optical coherence tomography.[1] The laser cavity consists of three components coupled in a short (10's of cm's) fiber cavity: a fiber-coupled polarization sensitive optical amplifier, a fiber tap, and a fiber Fabry-Pérot tunable filter. The amplifier and fiber tap are hybrid components that include integrated polarization-dependent isolators. The amplifier is constructed with an isolator at both the input and output ports, while the fiber tap contains a single isolator at the pass port. The laser architecture can take two forms depending on the location of the tap within the laser ring. Figure 1 illustrates these two configurations.

It has been shown experimentally and described theoretically that the optical amplifier broadens the instantaneous linewidth of the high-speed swept laser.[2] Following amplification, the spectrally filtered light from the FFP-TF experiences undesired spectral broadening. This effect requires that the designed 3 dB bandwidth of the FFP-TF be smaller than the desired system linewidth. This effect is greatest in the "amplifier last" configuration illustrated in Fig. 1(b). While the linewidth may increase, the output power is greater in the "amplifier last" configuration as compared to the "filter last" configuration since the signal is not subjected to the insertion loss of the FFP-TF immediately before the tap.

It is difficult to produce a high duty cycle, linear scan with these configurations alone. There is a non-zero amount of time required to return the filter passband to the start wavelength during which the laser either must lase or be turned off. If the amplifier remains powered on, the system generates both increasing and decreasing wavelength swept cycles with probable asymmetric results. If powered off, the system operates at < 50 % duty cycle. Utilization of an interleave optical circuit provides a number of key advantages when the laser ring is operated at < 50 % duty cycle.[1] One, each cycle on the output of the interleaver is comprised of a single sweep

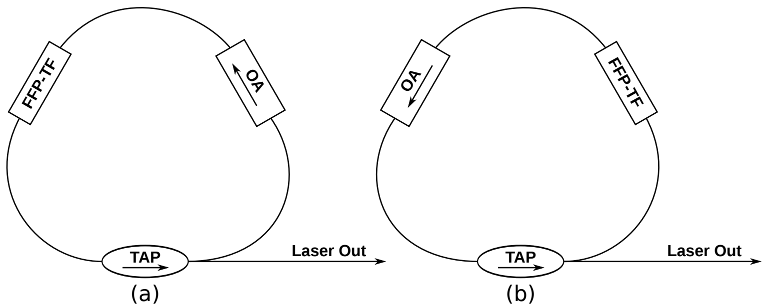

Figure 1. The all-fiber laser cavity can take two forms: "filter last" and "amplifier last". Laser power is coupled out immediately after the tunable filter (FFP-TF) (a) and after the optical amplifier (OA) (b). Arrows indicate the orientation of the isolators within those components that contain them.

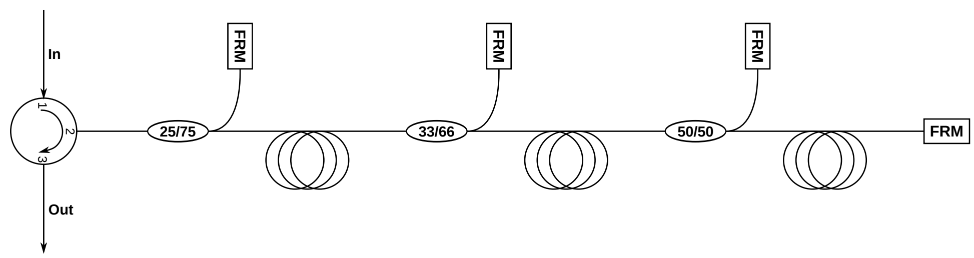

Figure 2. Optical interleaver circuit resulting in a 4x increase in sweep rate when coupled with a 25 % duty cycle swept-laser source. Circuit contains a circulator, fiber couplers (coupling ratios noted), fiber delay lines of 1026 m (for a 25 kHz native scan resulting in a 100 % duty cycle 100 kHz swept source), and Faraday rotator mirrors (FRM).

of increasing wavelength. Two, the linearity of the sweep cycle is significantly improved. Three, the sweep rate is increased by a factor proportional to the number of stages within the interleaver. And four, the system can lase at 100 % duty cycle. There are different interleaver circuit approaches.[3,4] Figure 2 illustrates the approach taken in this research. This specific configuration reduces the amount of fiber in the delay lines and the number of optical components compared to other interleaver designs. Figure 2 illustrates a design for a 25 % duty cycle, 25 kHz native scan, 100 kHz laser design. Other configurations are possible for differing duty cycles and native scan rates by adjusting the number of stages and fiber delay line length. When the fiber ring laser is operated at 25 % duty cycle, the ring can produce a single cycle of highly linear, increasing wavelength swept laser light. The optical interleaver circuit converts a single cycle, operating at 25 % duty cycle, into a 100 % duty cycle scan at four times the input rate. Thus, the circuit illustrated in Fig. 2 produces, from a 25 % duty cycle, 25 kHz native scan rate, a 100 % duty cycle, 100 kHz swept-source system.

2. DRIVING CIRCUITRY APPROACH

Traditionally, researchers in OCT laser sources have relied on the presence of a suitable mechanical resonance in the tunable filter component at which to natively scan the laser ring illustrated in Fig. 1. Manufacturers of these components have historically serviced telecommunication or sensing applications where scan rates are significantly smaller than the 10's or even 100's of kHz sweep rates desired by the OCT community. Current FFP-TF designs are not optimized for these sweep rates when relying on the existence of a mechanical resonance.

FFP-TF's devices often are designed around a piezoelectric component used to control the resonant cavity within the Fabry-Pérot etalon. Electrically, the component is mostly capacitive and can be modeled as such when operated away from the mechanical resonances of the device. This research presents a novel approach to driving the FFP-TF off mechanical resonance, reducing the high drive current required at high excitation frequencies. A bias-T network followed by a resonant tank circuit (a parallel LC circuit formed using the capacitive load of the FFP-TF) is a straightforward approach for driving the capacitive load of the FFP-TF at multi-kHz, off mechanical resonance, sweep rates. Figure 3 illustrates the circuits used in this research to drive the FFP-TF

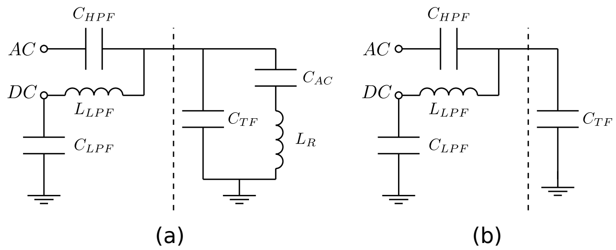

Figure 3. Schematic of the FFP-TF signal conditioning circuit. The AC coupling capacitors C_{HPF}, C_{LPF}, and C_{AC} are 1000 μF (a) Off mechanical resonance (10 kHz and 25 kHz). L_R is 18.4 μH at 25 kHz, and 115 μH at 10 kHz where the FFP-TF load, C_{TF}, is ≈ 2.2 μF. (b) On mechanical resonance (≈ 48 kHz). Left of the dashed line is the bias-T network (high pass filtered AC input and low pass filtered DC input). Right of the dashed line is the resonant tank circuit, where the FFP-TF is modeled as C_{TF}, (a), and the FFP-TF load in (b).

at off and on mechanical resonant frequencies. The bias-T operates over a wide range of input frequencies and is designed to work over the frequency range of interest in this research. The tank circuit resonance frequency, f_0, must be tuned to the desired native sweep rate of the laser ring by adjusting L_R. For example, a native scan rate of 25 kHz (100 kHz after a 4 stage interleaver) requires a parallel inductive load, L_R. Given the capacitive load of the FFP-TF of 2.2 μF (typical for a Micron Optics FFP-TF), L_R is calculated from the relationship

$$f_0 = \frac{1}{2\pi\sqrt{LC}} \tag{1}$$

as 18.4 μH. This circuit allows for the operation of the laser at multi-kHz sweep rates without the requirement of a strong mechanical resonance in the FFP-TF at that specific frequency or large drive current. Similarly, a native scan rate of 10 kHz requires a parallel inductive load of 115 μH. An AC coupling capacitor is required in series with the inductor to AC couple the DC bias signal. Variations of this circuit can be included to control the Q factor of the resonance in cases where tolerances of components can not offer precise control over the resonance, but sweep rates must be tightly controlled. In this research, Q factors were observed to be relatively small. The electrically resonant circuit in Fig. 3(a) could be driven within a few percent of the designed frequency without detrimental increases in drive current.

3. EXPERIMENTAL METHODOLOGY

Fiber Fabry-Pérot tunable filter-based swept-wavelength lasers have been used to create laser systems with sweep rates as high as 240 kHz and instantaneous output powers in excess of 100 mW.[1] A complete swept-wavelength laser system described in this manuscript, with a 4-stage interleaver, is illustrated in Fig. 4.

A system consists of three parts: the fiber ring laser, the N-stage interleaver, and the booster. The fiber ring laser, as discussed above, consists of three components and can take two forms as illustrated in Fig. 1. Both forms are considered. The N-stage interleaver consists of a circulator followed by $N-1$ fiber delay lines, $N-1$ fiber couplers of various coupling efficiencies, and N Faraday rotator mirrors. The ideal coupling efficiencies are calculated such that each delayed cycle of the input laser signal are equal in power.

This research investigates the following elements of a complete system configuration. Two laser configurations are considered as illustrated in Fig. 1: "filter last" and "amplifier last" configurations. Three native sweep rates are considered: 10 kHz, 25 kHz, and 50 kHz. Three duty cycles (or interleaver designs) are considered: 25 % (4-stage), 33 % (3-stage), and 50 % (2-stage). Finally, three different FFP-TF designs are considered with 3 dB bandwidths of ≈ 200 pm, ≈ 100 pm, and ≈ 75 pm operating at 1310 nm.

A major disadvantage of this system type is the necessity for a relatively large fiber-based cavity on the order or 10's of cm's, and, thus, large photon round trip time. This requirement limits the minimum bandwidth of the intra-cavity wavelength selective component (FFP-TF) and dictates the regime in which the laser is operating: saturation regime, multiple round trip regime, and single round trip regime.[5] In the saturation regime, the slew rate of the laser and the bandwidth of the FFP-TP are configured such that photons are able to propagate

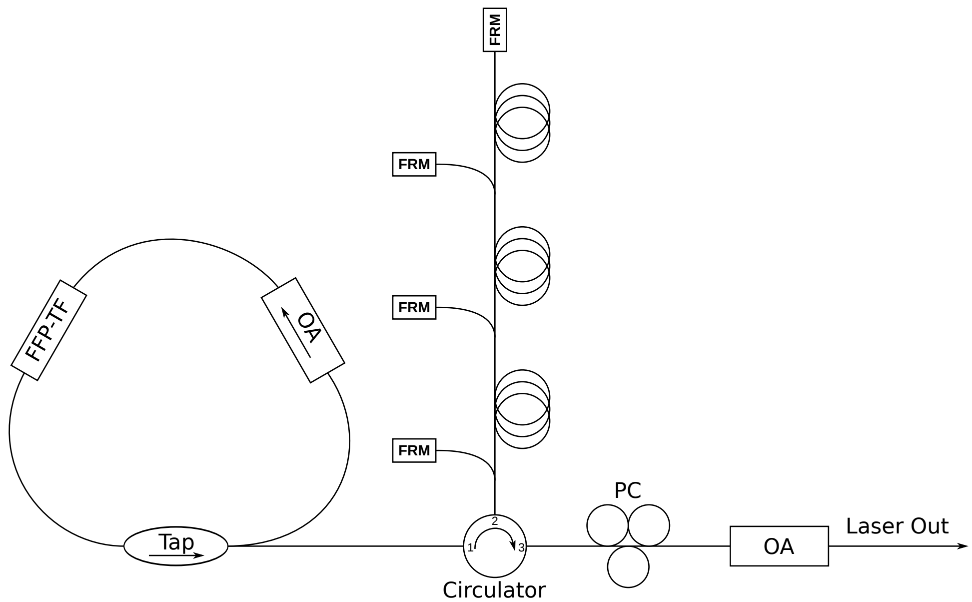

Figure 4. A complete laser system. It consists of a fiber ring laser (left), an 4-stage interleaver (middle), and a power booster (right). The power booster (OA) is polarization sensitive and requires a polarization controller (PC) to align the polarization state from the output of the interleaver to the input of the booster.

multiple times (typically > 10) around the laser cavity, and, as the name suggests, the gain medium is able to be driven into complete saturation. In the single round trip regime, the slew rate of the laser is configured to scan a wavelength span equal to the 3 dB bandwidth of the FFP-TF in the time it takes a photon to travel a single round trip within the laser cavity. The configurations in this research operate (mostly) within the multiple round trip regime which lies between the two. Within this regime, the laser can maintain a large sweep bandwidth, high output power, and high sweep rate.

The minimum required bandwidth of the FFP-TF is a function of the filter slew-rate. We can get a qualitative sense for the minimum bandwidth of the FFP-TF by calculating the number of laser cavity round trips, N_{RT}, a photon can propagate during the time FFP-TF slews a frequency range equal to the 3 dB bandwidth, $\Delta\lambda_{TF}$. Even at one round trip, a photon experiences an insertion loss of 3 dB, and, thus, the laser has a reduced output power. Given the total bandwidth span of the scanning laser, $\Delta\lambda_L$, the duty cycle, D, and scan frequency, f_0, of the native laser ring in Fig. 1, the number of cavity round trips, N_{RT}, can be approximated by the ratio of the time the filter slews the bandwidth of the FFP-TF, ΔT, to the round trip time of the laser cavity, ΔT_{RT} as

$$N_{RT} = \frac{\Delta T}{\Delta T_{RT}} = \frac{\Delta\lambda_{TF} D/(\Delta\lambda_s f)}{nL/c} = \frac{\Delta\lambda_{TF} Dc}{\Delta\lambda_s f n L} \ . \tag{2}$$

The number of permutations described above makes constructing a complete laser system for each configuration impractical. In practice, we consider each configuration in the following manner. The approach is illustrated in Fig. 5. A laser ring was constructed for each laser ring configuration and FFP-TF bandwidth combination using a Micron Optics FFP-TF and a ThorLabs Booster Optical Amplifier (small signal gain of ≈ 30 dB). When analyzing the complementary laser configuration, the laser ring splices were broken and the active components (FFP-TF and OA) re-spliced in the proper order with a new fiber tap. This approach avoided the need for additional high cost active components.

The DAQ system consists of the following components. An ATS9350 AlazarTech PCI digitizing card for capturing the signals from the balanced photoreceivers, a 33500B Agilent function generator for generating the sinusoidal AC signals and frequency coupled TTL signals for enabling the amplifiers at the proper phase within the scan, the FFP-TF signal conditioning circuit illustrated in Fig. 3, TEC controllers for both amplifiers, and

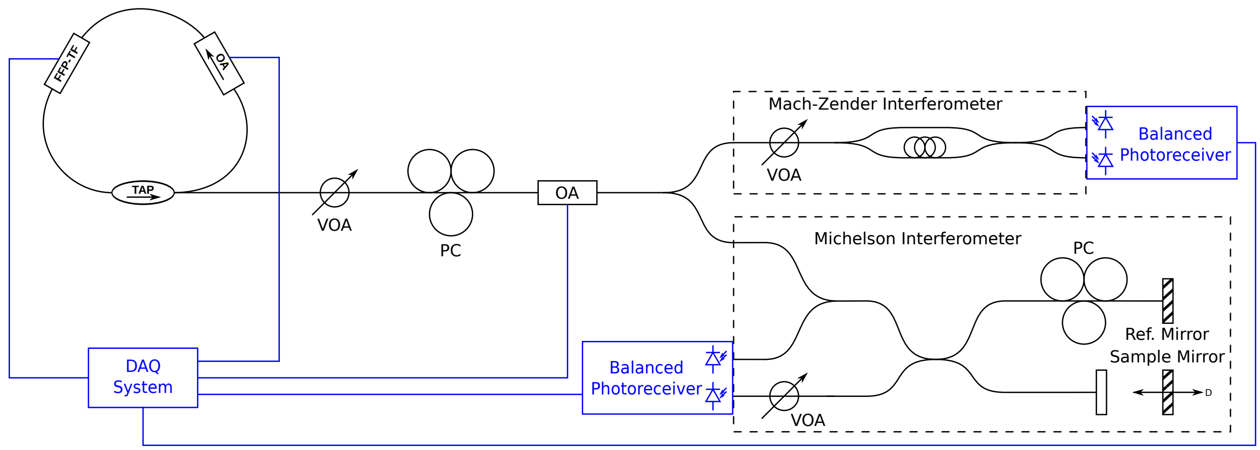

Figure 5. Experimental setup for investigating each laser system permutation. The setup consists of the laser ring, a variable optical attenuator (VOA) to model the losses incurred by the interleaver, a polarization controller (PC) used to align the polarization to the booster amplifier, a booster amplifier, a Mach-Zehnder interferometer for signal linearization, and a Michelson interferometer to measure the coherence length of the system.

Stages	Loss (dB)
2	13
3	10.5
4	7

Table 1. Approximate insertion loss experienced by each output cycle from the interleaver as compared to the input power level of the native scan.

a buffer op-amp for converting the output of the function generator and driving the AC input of the FFP-TF circuit.

As each laser ring configuration is constructed, the DAQ and fiber system is adjusted to operate at the desired native frequency (10 kHz, 25 kHz, or 50 kHz) and duty cycle (25 %, 33 %, or 50 %). A variable optical attenuator (VOA) at the output of the laser ring is adjusted to an attenuation equal to that of the interleaver that would be required for that duty cycle. For example, a 4 stage interleaver (25 % duty cycle laser configuration) introduces $\approx$ 13 dB loss to each output cycle of the input signal. Assuming a 0.5 dB insertion loss for each port of the circulator, and (for the first stage) a double pass through a 25 % coupler, the first cycle from the output of the interleaver is $\approx$ 13 dB lower than the input signal. Table 1 summarizes the loss approximations for each interleaver configuration. For a 3 stage interleaver (33 % duty cycle laser configuration), the attenuator is set to 10.5 dB. For a 2 stage interleaver (50 % duty cycle laser configuration), the attenuator is set to 7 dB.

The DAQ system is configured not only to pulse the inter-cavity amplifier within the laser ring, but also to drive the booster amplifier in an identical manner. This approach allows for a power measurement to be made at the output of the booster amplifier that is affected only by the single cycle of the interleaver that is being modeled and not by amplifier spontaneous emission (ASE) power that would otherwise not exist in a complete system. The polarization controller (PC) is adjusted to maximize the measured power at the output of the booster amplifier, thus ensuring that the input polarization is aligned with the input polarization axis of the booster amplifier.

The DAQ system is used to observe the interferogram measured at the output of a New Focus model 1817 balanced photo receiver from the 267 GHz Mach-Zehnder fiber-based interferometer. A VOA is used to keep the fixed gain photoreceiver from saturating and within the linear regime of the photoreceiver. The AC and DC signals of the FFP-TF signal conditioning circuit illustrated in Fig. 3 are adjusted to center the interference pattern within the data acquisition window as well as maximize the lasing span of the system. Practically, $\approx$ 20 dB fringe visibility is observed at the start and end of the scan as compared to the maximum contrast in the middle of the scan. Simultaneously, the sweep linearity is monitored and the phase offset of the amplifier enabled signals (in relation to the AC drive signal) generated by the function generator is adjusted to minimize the maximum observed non-linearity.

Once the system is adjusted and stable, a number of power and spectral measurements are made. A time-average power level is measured and recorded at the output of the laser ring, after the attenuator, and after the booster amplifier. With these power measurements, a measure of the amplifier gain (and level of saturation) is calculated. In addition, the output power of a complete system is estimated by multiplying the power levels measured by the number of stages of the required interleaver. Spectral measurements are made at the output of the laser ring and after the booster amplifier as well.

Table 3 in Appendix B summarizes the observations.

4. COMPLETE SYSTEM WITH CLOSED LOOP CONTROL

Drift and hysteresis characteristics of low voltage piezoelectric devices require that closed loop feedback control of the DC and AC signals be applied to the FFP-TF in order to maintain the desired sweep range of the laser. In this research we present an approach that utilizes two fiber Bragg gratings (FBG's) to lock to and maintain the desired sweep range. Two gratings are chosen within the wavelength span of interest. A fiber tap is used to couple a small amount of the laser power to a reference optical circuit. The optical signal is monitored from each FBG, and timing signals are generated and captured by a microprocessor. The microprocessor uses the timing signals to close the loop on both the AC and DC signals applied to the FFP-TF driving circuit to maintain the desired sweep range. Closed loop control provides both turn key operation as well as long term stability of the optical output; shortening the time between calibration cycles of the sweep nonlinearity. Figure 6 illustrates the reference optical circuit used for closed loop control. Two 1.5 nm bandwidth, high reflectivity (> 70 %) FBG's

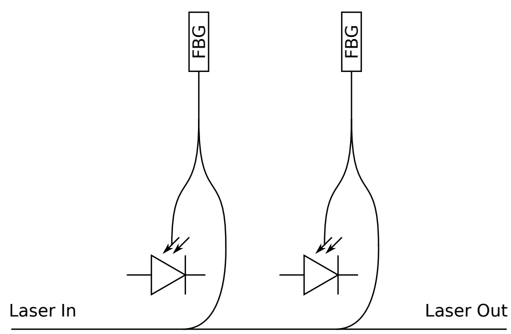

Figure 6. A simple reference circuit for closed loop control of a high speed swept-source laser system. The system consists of two low power taps (≈ 1 %) and two fiber Bragg gratings (FBG's). The reflective wavelengths of the FBG's are chosen to be at the extents of the desired laser scan.

are chosen at wavelengths at the extents of the laser scan of 1260 nm and 1340 nm. These wavelengths are well within the 150 nm lasing range capable of the optical amplifiers used in this research.

A complete system is constructed from a single configuration description. An "amplifier last", 25 kHz native scan, 25 % duty cycle (4 stage interleaver) laser ring configuration was constructed resulting in 100 kHz, 100 % duty cycle high speed swept source. The FFP-TF has a 3 dB bandwidth of ≈ 200 pm.

The system was able to achieve a 20 dB scan bandwidth of 165 nm from 1218 nm to 1383 nm. A time average power of 70 mW (18.5 dBm) was measured with 8.5 dB intra scan variation and only 0.35 dB inter scan variation. Peak instantaneous power was estimated at 108 mW (20.33 dBm). Using the Mach-Zehnder and Michelson interferometers of Fig. 5, a coherence length of 3.65 mm was measured. Spatial resolution (3 dB width) of < 10 μm was also observed. Figure 7 presents OCT images captured from a complete OCT system using this laser.

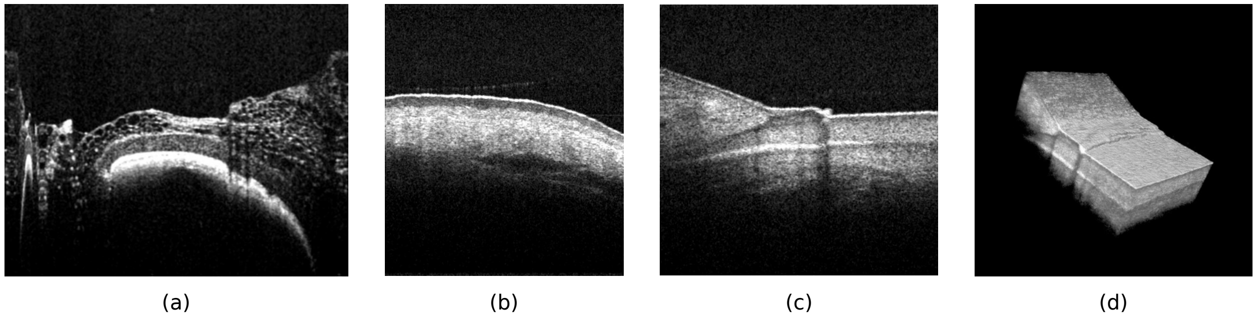

Figure 7. OCT system images of (a) cross-sectional image of a cucumber, (b) cross-sectional image of the epidermis and dermis of a human finger, (c) cross-section image and (d) 3-D reconstruction of a human nail fold. Swept-wavelength laser is described in section 4 and used with an OCT imaging system design by and located at Brett Bouma's group at the Wellman Center for Photomedicine at Massachusetts General Hospital.

	Coherence Length (mm)		
3 dB Linewidth (pm)	Lorentzian	Gaussian	Sinc-Squared
200	5.9	7.6	7.6
100	11.8	15.1	15.2
75	15.7	20.2	20.3

Table 2. Theoretical coherence lengths for three line shapes (Lorentzian, Gaussian, and sinc-square) calculated for the bandwidths of the three FFP-TF used in the research.

5. RESULTS AND CONCLUSION

The FFP-TF provides a nearly Lorentzian passband. Without nonlinear processes imparted by the optical amplifier within the ring (when in the configuration illustrated in Fig. 1(a))[2] and without a booster amplifier, the line shape of the laser follows closely the passband of the filter. The coherence length* can be estimated in theory. Given a Lorentzian line shape, the 3 dB bandwidth ($\Delta\lambda_{TF}$) is related to the coherence length (L_c) by

$$L_c \approx 0.688 \frac{\lambda^2}{\Delta\lambda_{TF}} \ . \tag{3}$$

Similar relationships exist for Gaussian line shapes,

$$L_c = \frac{4 \ln 2}{\pi} \frac{\lambda^2}{\Delta\lambda_{TF}} \ , \tag{4}$$

and even a sinc-squared line shape (square pulse of light) as

$$L_c \approx 0.8859 \frac{\lambda^2}{\Delta\lambda_{TF}} \ . \tag{5}$$

Table 2 summarizes the theoretical coherence lengths for these line shapes given the bandwidth of the FFP-TF's used in this research. The results summarized in Table 3 highlight a number of interesting aspects of the design. A wide range of coherence lengths were observed within each subset of data for each FFP-TF. For instance, the 200 pm FFP-TF exhibited coherence lengths ranging from 4.064 mm to 9.652 mm. The trend to higher coherence length followed the hypotheses set out in this research in that the "amplifier last" laser ring configuration results in a laser with a line shape larger than the FFP-TF within the ring. Given a theoretical limit of 5.9 mm to 7.6 mm, the data aligns quite well with results. It is important to note that the bandwidth of a FFP-TF is a

*Coherence length in this paper is defined as the total distance over which the contrast of the interferogram is < 3 dB the contrast at zero path difference. See Appendix A.

function of wavelength and not necessarily constant over the operating band. Future measurements could be performed that would quantify the coherence length as a function of wavelength in contrast to the system as a whole.

The 100 pm FFP-TF exhibited coherence lengths ranging from 7.112 mm to 20.32 mm, while the 75 pm FFP-TF exhibited coherence lengths ranging from 10.16 mm to 23.37 mm. Again, we observe trends that the "filter last" configuration produces swept-sources with higher coherence lengths.

As mentioned early, the coherence length is greater in the "filter last" configuration but less of output power. On average, the 200 pm FFP-TF configurations experienced 2.1 dB power loss, the 100 pm FFP-TF configurations experienced 2.2 dB power loss, and the 75 pm FFP-TF configurations experienced 1.6 dB power loss. The extent of the power loss is minimized due to the fact that the booster amplifier is operating in high saturation. Higher input powers experience less gain as do lower input powers. Booster gains are measured as low as only 16 dB in "amplifier last" configurations compared to some "filter last" configurations that experience near small signal gain of 30 dB.

The complete laser system described in Section 4 compares well to the data collected and summarized in Table 3. The complete system measured a coherence length of 3.65 mm and output power of 18.45 dBm (70 mW). An identically defined system analyzed in Section 3 measured a coherence length of 4.572 mm and estimated system output power of 19 dBm. The experimental methodology utilized correlated well with the complete system results.

A few specific configurations stand out among the system permutations listed in Table 3. There exist multiple configurations of 100 and 200 kHz sweep rates with output powers > 18.5 dBm (70 mW) and 20 dB bandwidth of > 100 nm. An "OA last" configuration, scanning at 200 kHz (50 kHz native scan with 4 stage interleaver) produces a 150 nm 20 dB bandwidth scan with output power of 19.73 dBm (94 mW) with a coherence length of 4 mm. These and similar configurations maximize sweep speed and output power.

Configurations that maximize coherence exist as well. All "filter last" configurations operating at native scan speeds of 10 kHz with the 75 pm bandwidth FFP-TF produced laser sources with > 20 mm coherence length. The configuration running at 10 kHz native scan rate and 25 % duty cycle exhibits high output power of 19 dBm (80 mW) and a coherence length of 23.4 mm. This design would required three fiber delay lines of length 2566 m. If maximum system size prohibited this amount of fiber within the design, the laser could simply be operated without an interleaver, at 25 % duty cycle, and still maintain a time average output power of 13 dBm (20 mW).

6. SUMMARY

In this research we have developed a robust platform for configuring, testing, and deploying a high speed swept-wavelength laser source. It includes an all fiber swept-wavelength laser, a multi-stage interleaver, booster amplification, and reference components. In addition to the optical components, the complete system includes a single integrated circuit board and provides not only mechanical stability for the optical components, but all of the required electrical hardware (microprocessor, optical to electrical conversion, power supplies, FFP-TF driving circuitry, etc.) for stand alone, turn-key, stable operation. We have presented a brief outline of the platform used in this research with specific details for a 100 kHz laser design. In addition, a short summary of some initial results are also presented that match well with theory. We presented specific experimentally measured performance data on additional configurations (sweep range, sweep speed, laser configuration, with and without booster) optimizing and aiming for increasing coherence length and power.

While some of the configurations analyzed here are less feasible than others (due to long delay lines), the FFP-TF is shown to be a significant and agile component of a robust swept source platform for analyzing and characterizing system configurations. The single round trip regime was approached when operating the filter at mechanical resonance with the 75 pm bandwidth FFP-TF. From Eq. 2, it is estimated that $N_{RT} < 2$ round trips were being completed. With cavity lengths of ≈ 0.5 m, the design is close to the lower limit of filter bandwidths for this configuration. However, at the highest coherence lengths achieve here (10 kHz native scan rate with the 75 pm bandwidth FFP-TF), $N_{RT} > 7$. This result implies that larger coherence lengths for these configurations are possible. While required delay line lengths are long for these configurations, operating this system without an interleaver is possible at the expense of < 50 % duty cycles.

APPENDIX A. COHERENCE LENGTH AND IMAGING DEPTH

It is important to define coherence length in the context of this manuscript. Conceptually, the coherence of a light source describes the degree of correlation between two packets of light. These packets of light may or may not originate from the same source. When originating from a single source (as many interference experiments do), these packets of light may differ spatially or temporally. In any case, the degree at which constructive and/or destructive interference can be observed is characterized by the coherence of the light source.[6,7]

Coherence can be quantified by observing the contrast of fringe patterns generated from a light source of interest as a function of the spatial or temporal separation of the two light packets or paths. In the context of OCT, temporal separation is of more interest. In OCT, the laser source is often generated in a fiber-based laser where the fiber delivery system is single (spatial) mode. Spatial coherence in this context is considered to be large and not a limiting factor. Coherence length quantifies the extent in space over which the fringe visibility, or contrast, is one half the maximum fringe visibility observed at zero path length difference. This definition is important to understand as it has consequences as to how OCT imaging depth is determined.

Imagine a fiber-based Mach-Zehnder interferometer composed of splitter, two adjustable lengths of fiber, and a combiner. A swept-source laser excites the input of the interferometer and the time-varying intensity of the output is recorded by a photodetector. Using the previous description, the coherence length can be defined as

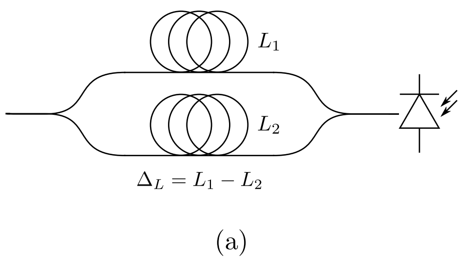

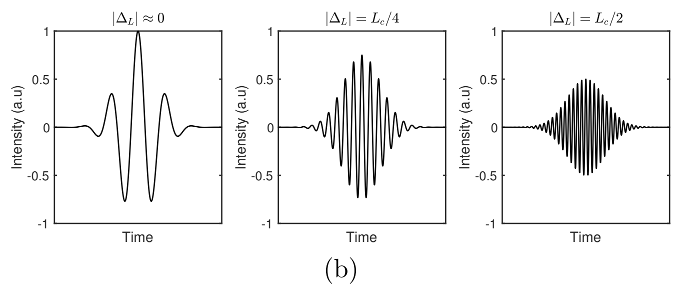

Figure 8. (a) Fiber-based Mach-Zehnder interferometer. (b) Measured intensity of a swept-source laser at the output of (a) with three difference path differences. At near zero-path length difference ($|\Delta L| \approx 0$), the fringe contrast is at a maximum (1 a.u.). As the path length difference increases, the fringe contrast decreases to 0.5 at $|\Delta L| = L_c/2$.

the total distance (path length difference) at which the fringe contrast is greater than or equal to the maximum contrast at zero path length difference. The interferometer in Fig. 8(a) exhibits a fringe contrast of 0.5 at two conditions: $L_2 - L_1 = L_c/2$ and $L_1 - L_2 = L_c/2$, or $\Delta_L = \pm L_c/2$.

In optical frequency domain imaging (OFDI), a version of the Michelson interferometer is often used to image scattering media (such as biological tissue). Each scatter represents a discrete reflection for which a periodic interferogram is detected at the output of the interferometer. Figure 9 illustrates a simplified version of this

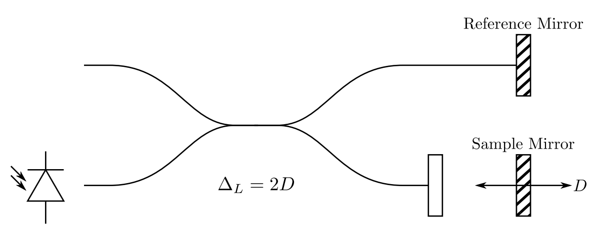

Figure 9. Michelson interferometer. The total path length difference, Δ_L, is twice the sample mirror displacement, D, from the zero path length difference location (shown).

configuration. Due to the nature of an OCT measurement in that light must travel twice the depth to the imaged scatterer, the effective imaging distance is one half the coherence length as defined above. In addition, there is a depth degeneracy present in all interferometric measurement systems. One cannot determine whether $L_1 > L_2$

or $L_2 > L_1$ in the case of the Mach-Zehnder interferometer in Fig. 8 or whether $D > 0$ or $D < 0$ in the case of the Michelson interferometer in Fig. 9. In this case, the effective imaging distance could be defined as being only one quarter of the coherence length as defined above. The depth degeneracy problem has been solved and most modern OCT systems utilize a technique to overcome the depth degeneracy.[8,9] Thus, given the coherence length, L_c, the effective imaging depth is defined as one half the coherence length.

In this paper we cite two numbers when characterizing the coherence of the swept sources: the coherence length, L_c, and the effective imaging depth, D_i. These parameters have the following relationship:

$$D_i = \frac{L_c}{2} \ . \tag{6}$$

APPENDIX B. SUMMARY OF RESULTS

Table 3 summarizes the observations in this research. The data describes each system configurations analyzed and the observed power levels, spectral profiles, and coherence lengths of each as described in 3.

System Parameters					After Ring		After Booster				
System Scan Speed (kHz)	Native Scan Speed (kHz)	Native Duty Cycle (%)	FFP-TF BW (pm)	Laser Ring Config.	Power (dBm)	20 dB BW (pm)	Power (dBm)	20 dB BW (pm)	Booster Gain (dB)	Est. System Power (dBm)	$L_c(mm)$
40	10	25	200	Filter Last	0.8	188	11.06	186	23.26	17.06	9.652
30	10	33	200	Filter Last	1.8	194	13.37	192	22.07	18.07	9.652
20	10	50	200	Filter Last	3.7	178	15.51	178	18.81	18.51	9.144
100	25	25	200	Filter Last	0.5	180	11.9	177	24.4	17.9	7.11
75	25	33	200	Filter Last	1.5	178	13.4	188	22.4	18.1	6.604
50	25	50	200	Filter Last	2.8	182	14.973	182	19.173	17.973	6.096
200	50	25	200	Filter Last	-6.8	159	9.38	164	29.18	15.38	4.064
150	50	33	200	Filter Last	-4.06	163	11.9	162	26.46	16.6	4.3688
100	50	50	200	Filter Last	-0.8	166	14.48	166	22.28	17.48	4.064
40	10	25	200	OA Last	5.57	170	13.37	168	20.8	19.37	7.112
30	10	33	200	OA Last	6.4	180	14.8	175	18.9	19.5	7.112
20	10	50	200	OA Last	7.7	174	16.65	173	15.95	19.65	7.112
100	25	25	200	OA Last	5.5	171	13.04	167	20.54	19.04	4.572
75	25	33	200	OA Last	6.45	170	14.7	168	18.75	19.4	4.064
50	25	50	200	OA Last	7.6	173	16.6	172	16	19.6	4.064
200	50	25	200	OA Last	5	152	13.73	150	21.73	19.73	4.064
150	50	33	200	OA Last	5.9	163	15.16	161	19.76	19.86	4.064
100	50	50	200	OA Last	7.18	169	16.88	168	16.7	19.88	4.064
40	10	25	100	Filter Last	0.37	173	12.84	170	25.47	18.84	17.78
30	10	33	100	Filter Last	1.65	173	14.48	172	23.33	19.18	18.288
20	10	50	100	Filter Last	3.7	167	16.7	167	20	19.7	17.78
100	25	25	100	Filter Last	0.45	166	13.2	166	25.75	19.2	18.288
75	25	33	100	Filter Last	1.3	172	14.45	170	23.65	19.15	18.4912
50	25	50	100	Filter Last	2.83	168	15.47	168	19.64	18.47	17.78
200	50	25	100	Filter Last	-7.2	102	10.8	ASE	31	16.8	10.16
150	50	33	100	Filter Last	-3.6	104	14.8	ASE	28.9	19.5	10.16
100	50	50	100	Filter Last	0.1	100	17.3	101	24.2	20.3	10.3632
40	10	25	100	OA Last	5.8	176	14.74	174	21.94	20.74	10.16
30	10	33	100	OA Last	6.9	176	16.25	173	19.85	20.95	11.48
20	10	50	100	OA Last	8.2	171	17.55	171	16.35	20.55	13
100	25	25	100	OA Last	5.9	169	14.82	168	21.92	20.82	7.112
75	25	33	100	OA Last	6.8	175	16.23	172	19.93	20.93	7.62
50	25	50	100	OA Last	8.2	170	18.11	169	16.91	21.11	5.588
200	50	25	100	OA Last	6.3	103	15.75	102	22.45	21.75	13.208
150	50	33	100	OA Last	7.6	100	17.34	100	20.24	22.04	18.288
100	50	50	100	OA Last	9.1	101	19.26	101	17.16	22.26	20.32
40	10	25	75	Filter Last	0.2	161	13.04	160	25.84	19.04	23.368
30	10	33	75	Filter Last	1.36	160	14.79	161	23.93	19.49	22.86
20	10	50	75	Filter Last	2.9	165	16.55	164	20.65	19.55	22.86
100	25	25	75	Filter Last	0.05	159	13.1	162	26.05	19.1	20.828
75	25	33	75	Filter Last	1.44	160	14.93	159	23.99	19.63	22.352
50	25	50	75	Filter Last	2.58	160	16.7	160	21.12	19.7	21.336
200	50	25	75	Filter Last							
150	50	33	75	Filter Last							
100	50	50	75	Filter Last							
40	10	25	75	OA Last	4.6	168	14.67	160	23.07	20.67	14.224
30	10	33	75	OA Last	5.8	158	16.36	154	21.06	21.06	15.24
20	10	50	75	OA Last	7.17	156	18.23	156	18.06	21.23	17.272
100	25	25	75	OA Last	4.85	153	14.82	152	22.97	20.82	14.224
75	25	33	75	OA Last	5.66	163	16.28	159	21.12	20.98	10.16
50	25	50	75	OA Last	7	157	18.27	157	18.27	21.27	10.668
200	50	25	75	OA Last							
150	50	33	75	OA Last							
100	50	50	75	OA Last							

Table 3. Summary of results for 54 permutations of the laser system characteristics. When "ASE" is noted in the 20 dB BW column, the ASE level is higher than 20 dB from the maximum level. Blank columns signify that the system configuration was unstable and operating in the single round trip regime.

ACKNOWLEDGMENTS

Special thanks goes to Norman Lippok, Sahar Hosseinzadeh Kassani, and the rest of Brett Bouma's group at the Wellman Center for Photomedicine at Massachusetts General Hospital for their advice, collaboration, and use of their facilities.

REFERENCES

[1] Jun, C., Villiger, M., Oh, W.-Y., and Bouma, B. E., "All-fiber wavelength swept ring laser based on Fabry-Pérot filter for optical frequency domain imaging," *Opt. Express* **22**, 25805–25814 (Oct 2014).

[2] Lippok, N. and Bouma, B. E., "Self-phase modulation induced spectral broadening in wavelength swept SOA fiber ring lasers," *Photonics West* (Feb. 2016).

[3] Schlachter, S. C., Kang, D., Gora, M. J., Vacas-Jacques, P., Wu, T., Carruth, R. W., Wilsterman, E. J., Bouma, B. E., Woods, K., and Tearney, G. J., "Spectrally encoded confocal microscopy of esophageal tissues at 100 khz line rate," *Biomed. Opt. Express* **4**, 1636–1645 (Sep 2013).

[4] Wieser, W., Biedermann, B. R., Klein, T., Eigenwillig, C. M., and Huber, R., "Multi-megahertz oct: High quality 3d imaging at 20 million a-scans and 4.5 gvoxels per second," *Opt. Express* **18**, 14685–14704 (Jul 2010).

[5] Huber, R., Wojtkowski, M., Taira, K., Fujimoto, J. G., and Hsu, K., "Amplified, frequency swept lasers for frequency domain reflectometry and oct imaging: design and scaling principles," *Opt. Express* **13**, 3513–3528 (May 2005).

[6] Born, M. and Wolf, E., [*Principles of optics : Electromagnetic theory of propagation, interference and diffraction of light*], Cambridge University Press, New York, New York (1999).

[7] Hecht, E., [*Optics*], Addison-Wesley, Reading, Mass. (2002).

[8] Yun, S. H., Tearney, G. J., de Boer, J. F., and Bouma, B. E., "Removing the depth-degeneracy in optical frequency domain imaging with frequency shifting," *Opt. Express* **12**, 4822–4828 (Oct 2004).

[9] Vakoc, B. J., Yun, S. H., Tearney, G. J., and Bouma, B. E., "Elimination of depth degeneracy in optical frequency-domain imaging through polarization-based optical demodulation," *Opt. Lett.* **31**, 362–364 (Feb 2006).